AGN-Induced Cavities in NGC 1399 and NGC 4649

K. Shurkin[1], R.J.H. Dunn[2], G. Gentile[1], G.B. Taylor[1], and S.W. Allen[3]

[1] University of New Mexico, Department of Physics and Astronomy, Albuquerque, NM 87131, USA.
[2] School of Physics and Astronomy, University of Southampton, Southampton, SO17 1BJ, UK.
[3] Kavli Institute for Particle Astrophysics and Cosmology, Stanford University, 382 Via Pueblo Mall, Stanford, CA 94305-4060, USA.

16 November 2007

ABSTRACT

We present an analysis of archival *Chandra* and VLA observations of the E0 galaxy NGC 1399 and the E2 galaxy NGC 4649 in which we investigate cavities in the surrounding X-ray emitting medium caused by the central AGN. We calculate the jet power required for the AGN to evacuate these cavities and find values of $\sim 8 \times 10^{41}$ erg s^{-1} and $\sim 14 \times 10^{41}$ erg s^{-1} for the lobes of NGC 1399 and $\sim 7 \times 10^{41}$ erg s^{-1} and $\sim 6 \times 10^{41}$ erg s^{-1} for those of NGC 4649. We also calculate the k/f values for each cavity, where k is the ratio of the total particle energy to that of electrons radiating in the range of 10 MHz to 10 GHz, and f is the volume filling factor of the plasma in the cavity. We find that the values of k/f for the lobes of NGC 1399 are ~ 93 and ~ 190, and those of the lobes of NGC 4649 are ~ 15000 and ~ 12000. We conclude that the assumed spectrum describes the electron distribution in the lobes of NGC 1399 reasonably well, and that there are few entrained particles. For NGC 4649, either there are many entrained particles or the model spectrum does not accurately describe the population of electrons.

Key words: galaxies: active — galaxies: nuclei — galaxies: individual: NGC 1399 — galaxies: individual: NGC 4649 — radio continuum: galaxies — X-rays: galaxies

1 INTRODUCTION

Within nearby galaxies, groups, and clusters, embedded active galactic nuclei (AGN) have been found to interact with the surrounding hot, X-ray emitting thermal gas, causing such disturbances as shocks, ripples, and cavities (e.g. Fabian et al. 2000, 2003, 2006; Forman et al. 2005). The cavities, which appear as X-ray surface brightness depressions, consist of low density relativistic plasma and are a consequence of the thermal gas being displaced by the jets of the AGN. They have been found to be associated with the central AGN of many clusters, such as Perseus (Böhringer et al. 1993; Fabian et al. 2000, 2003, 2006), Hydra A (McNamara et al. 2000), M 87 (Churazov et al. 2001; Forman et al. 2005), and Centaurus (Taylor et al. 2002, 2006). AGN-induced disturbances are also present within the hot interstellar medium (ISM) in the haloes of normal elliptical galaxies (Diehl & Statler 2006). Many early-type galaxies, such as M 84 (Finoguenov & Jones 2001), have been found to harbor cavities in their X-ray haloes. Our interest in these AGN-induced cavities stems from the fact that they can be used as calorimeters. The kinetic energy of the jets emanating from the central black hole can be estimated by calculating the amount of energy required to inflate the observed cavities (Bîrzan et al. 2004; Rafferty et al. 2006; Dunn & Fabian 2006). Using this estimate, the jet power can be calculated once an approximate age of the cavity has been deduced.

For nearby large, elliptical galaxies, accurate measurements of the density and temperature profiles of the thermal gas can be ob-

tained from high resolution *Chandra* observations. For those systems that are sufficiently close, such that radii within an order of magnitude of the accretion radius are resolved, these measurements can be used to calculate the Bondi accretion rate, given estimates of the black hole mass. Allen et al. (2006), in a study of 9 X-ray luminous sources that harbor cavities, found that a tight physical correlation exists between the power available from Bondi accretion of the hot gas and the observed jet power. These results are significant, especially for studies of accretion and jet formation, as well as the formation and evolution of galaxies. In particular, building upon earlier studies by Di Matteo et al. (2003) and Taylor et al. (2006), they confirmed that the bulk of the energy produced by the central AGN in these systems, which are all Fanaroff & Riley (1974) type-I sources, is released in the relativistic jets. The energy injected back into the environment is in principle sufficient to balance radiative cooling of the hot X-ray gas. This possibility has also been investigated by Best et al. (2005, 2006), who showed that the cooling of hot gas from the atmosphere of the host galaxy can feasibly provide the fuel for low power, radio-loud AGN, and that the heating by AGN feedback can balance this cooling, except perhaps in the most massive clusters. However, the manner in which the energy provided by the AGN is coupled to the thermal energy of the hot gas in order to offset cooling, as well as the efficiency of this process, are as yet unknown.

Because of the significance of AGN activity, it is desirable to investigate further the population of galaxies which exhibit interactions between the central AGN and the surrounding medium. In

particular, we are interested in those sources which harbor cavities, as they offer insight into the physical properties of the AGN itself.

We analyzed *Chandra* and VLA[1] data for NGC 1399 and NGC 4649, both of which are large, elliptical galaxies that harbor cavities and are located in nearby clusters. Because of their proximity, we are able to determine the density of the X-ray emitting gas down to radii within a factor of 10 of the accretion radius, making these two galaxies ideal for future analysis concerning Bondi accretion. At present, we use the cavities in these systems to estimate the kinetic energy of the jets and jet power. We also investigate the particle content of the cavities by determining k/f, where k is the ratio of the total particle energy contained in the cavity to the energy accounted for by electrons emitting synchrotron radiation in the range of 10 MHz to 10 GHz, and f is the volume filling factor of the relativistic plasma in the cavity. The cavities are filled with relativistic charged particles and magnetic fields, which together determine the synchrotron emission from the lobes. The relative energy densities of these two components, and hence k and f, cannot be disentangled from the emission alone. We must therefore consider the ratio k/f, which, under the assumption that the gas pressure is equal to the total pressure from the radio plasma, can be related to the magnetic field strength. The maximum field strength is obtained for the minimum value of $k/f = 1$, and would indicate a pure electron-positron plasma uniformly filling the cavity.

Our discussion will proceed as follows. We begin in §2 by describing the radio data selection and processing. In §3, we describe the X-ray data and preparation, as well as the identification of cavities. In §4 we present *Chandra*/VLA comparisons for NGC 1399 and NGC 4649 and determine the power of the jets in these systems. We present the k/f ratios in §5, followed by conclusions in §6.

Throughout this discussion, we assume a flat ΛCDM cosmology with $\Omega_M = 0.3$ and $H_0 = 70$ km s^{-1} Mpc^{-1}.

2   RADIO DATA: REDUCTION AND IMAGING

The VLA radio data were obtained from the NRAO archive. In selecting the data to be analyzed, preference was given to observations with time on source $\geqslant 5$ minutes. Because steep spectrum emission is brighter at lower frequencies, preference was also given to observations performed at 1.4 GHz. In addition, A-configuration or B-configuration observations at 1.4 GHz were desirable in order to provide arcsecond resolution for comparison with X-ray images from *Chandra*. Parameters for the VLA observations of NGC 1399 and NGC 4649 are tabulated in Table 1.

The radio data were reduced in the standard manner using AIPS. After an initial editing of the data, absolute amplitude and phase calibration were performed on each dataset using the scripts VLAPROCS and VLARUN. As the flux calibrator for each dataset was resolved, a model was used for the calibration. If bad data were still present after the initial calibration, those data were flagged and the calibration was repeated.

Each source was imaged using the task IMAGR. Sidelobes from outlying sources were removed by using multiple facets while imaging. Proper placement of the facets was determined using the task SETFC, which was set up to search a 0.5 degree radius for

sources in the NVSS[2] catalogue with flux $\geqslant 10$ mJy. Typically, sources outside of that range are either not bright enough or too far from the pointing center to have an appreciable effect on the quality of the image. As both sources had sufficient signal-to-noise ratios, imaging and phase-only self-calibration were then performed iteratively, until the theoretical noise was reached or until the quality of the map ceased to benefit from the iterations. Radio flux density measurements are shown in Table 2.

3   X-RAY DATA PREPARATION

The *Chandra* X-ray data were used to determine the deprojected temperature and density profiles of the X-ray emitting gas in the galaxies. These profiles, in combination with the measured sizes of the cavities identified from the X-ray and radio emission, allow the $P\,dV$ work done by the cavity on the surrounding gas halo to be calculated. The details of the X-ray observations are summarized in Table 1.

Before analysis, the X-ray data were reprocessed and cleaned using the CIAO software and calibration files (CIAO v3.3, CALDB v3.2). We began the reprocessing by removing the afterglow detection and re-identifying the hot pixels and cosmic ray afterglows, followed by the tool ACIS_PROCESS_EVENTS to remove the pixel randomization and to flag potential background events for data observed in Very Faint (VF) mode. The Charge-Transfer Inefficiency (CTI) was corrected for, followed by standard grade selection. Point sources were identified using the WAVDETECT wavelet-transform procedure. As these two galaxies were observed with the ACIS-S3 chip, background lightcurves to check for flaring were taken from the ACIS-S1 chip. For the spectral analysis, backgrounds were taken from the CALDB blank-field datasets. They had the same reprocessing applied, and were reprojected to the correct orientation.

Spectra were extracted in annular regions centered on the peaks of the X-ray emission from the galaxies. Annular regions were automatically assigned with constant signal-to-noise, stopping where the background subtracted surface brightness became consistent with zero. The initial signal-to-noise was 100, and this was increased or decreased by successive factors of $\sqrt{2}$ to obtain a number of regions between four and ten. The minimum signal-to-noise allowed was 10.

The $0.5 - 7$ keV spectra were extracted, binned with a minimum of 20 counts per bin, and, using XSPEC (v12.3.0) (e.g. Arnaud 1996), a PROJCT single temperature MEKAL (e.g. Mewe et al. 1995) model with a PHABS absorption was used to deproject the cluster. The deprojected cluster temperature, abundance and normalization profiles allowed the calculation of density and pressure profiles. Chi-square was used as the estimator in the fits.

These profiles give azimuthally averaged values for the cluster properties and have been used in the subsequent calculations. The substructure present in these galaxies is not expected to bias the results on the gas properties significantly (Donahue et al. 2006). As such the use of these azimuthally averaged values is not likely to introduce large biases into the subsequent calculations.

---

[1] The VLA (Very Large Array) is operated by the National Radio Astronomy Observatory (NRAO).

[2] The NVSS (NRAO VLA Sky Survey) is a 1.4 GHz continuum survey covering the entire sky north of -40° declination (Condon et al. 1998).

Table 1. Positions, redshifts, and radio and X-ray observation details for NGC 1399 and NGC 4649. The frequency (in GHz), configuration, date, and duration (in s) of the VLA observations are shown in columns 5 through 8. The ObsID and final exposure time (in ks) of the *Chandra* observations are shown in columns 9 and 10.

Source	RA[1] (J2000)	Dec[1] (J2000)	Redshift[1]	VLA Frequency (GHz)	Config	Date	Duration (sec)	CHANDRA ObsID	Exposure[2] (ks)
NGC 1399	03h 38m 29.08s	−35d 27m 02.7s	0.004753	1.465	H[3]	1983 Dec 16	27910	319	55.9
NGC 4649	12h 43m 39.66s	+11d 33m 09.4s	0.003726	1.465	B	1984 Jan 24	4410	785	36.9

[1] Positions and redshifts obtained from the NASA/IPAC Extragalactic Database (NED).
[2] The exposure after reprocessing.
[3] Hybrid configuration (A and B).

Table 2. Radio flux density measurements

Source	Peak Flux (Jy beam^{-1})	Total Flux Density (Jy)	RMS (μJy beam^{-1})	Beam (arcsec^2)	PA (deg)
NGC 1399	1.89×10^{-2}	4.63×10^{-1}	72.1	4.15×2.80	38.5
NGC 4649	1.72×10^{-2}	2.82×10^{-2}	29.7	4.51×3.64	44.8

Table 3. Properties

	NGC 1399	NGC 4649
Distance (Mpc)	19.4	17.1
L_{x} (erg s^{-1})*	4.27×10^{41}	1.91×10^{41}
$P_{1.4}$ (erg s^{-1} Hz^{-1})†	2.09×10^{29}	9.87×10^{27}
Scale (kpc arcmin^{-1})	5.64	4.96
Largest angular size (arcsec)‡	233	46.5
Largest physical size (kpc)‡	21.9	3.85

* X-ray luminosity, from O'Sullivan et al. (2001).
† Total isotropic radio power at 1.4 GHz: $P_{1.4} = 4\pi D^2 S_{1.4}$.
‡ Radio source size.

## 4 INTERACTION BETWEEN AGN JETS AND THERMAL GAS

In order to investigate any possible interactions between the AGN and the surrounding thermal gas, we superimposed the VLA radio contours onto the *Chandra* X-ray images. These X-ray/radio overlays are shown in Figures 1 and 2. Panels (a) and (b) of each figure show an adaptively smoothed X-ray image and an unsharp-masked X-ray image, respectively, with color scales chosen to highlight faint features. The adaptive smoothing was done with a 2 arcsec kernel up to a maximum of 20 using ASMOOTH (Ebeling et al. 2006). The unsharp-masked images are difference images made by first smoothing the raw image using a large Gaussian kernel (80 arcsec for NGC 1399 and 20 arcsec for NGC 4649), and then subtracting that image from one which has been smoothed using a 4 arcsec Gaussian kernel. The radio contours aid in the determination of the approximate size and location of the cavities. We use these estimates, in conjunction with density and temperature profiles derived from the X-ray data, to estimate the jet power required to inflate the observed cavities. These calculations are summarized in §4.3, following individual discussions of NGC 1399 and NGC 4649 in §4.1 and §4.2, respectively. Some additional derived properties of the galaxies are presented in Table 3.

4.1 NGC 1399

NGC 1399 is the central E0 galaxy of the Fornax cluster. It is host to a low power radio source, whose lobes are confined within the optical galaxy. Paolillo et al. (2002) present a ROSAT/VLA comparison which shows interactions between the central AGN and the surrounding hot gas. Figure 1 shows our *Chandra*/VLA comparison for NGC 1399. These comparisons confirm the structures found in Paolillo et al. (2002), as well as the presence of cavities associated with the radio lobes. The lobes extend north and south along an axis oriented ∼10 degrees west of north. They are approximately symmetric, each having a length of roughly 11 kpc. The central X-ray source is elongated in the direction of the lobes, with bulges along the east and west edge of the northern and southern lobes, respectively (see Figure 1b). The southern lobe bends sharply west before gradually bending eastward. As can be seen in Figure 1(a), a bright rim of X-ray emission follows the western edge of the southern lobe, marking the edge of the cavity. The northern lobe also bends slightly eastward at the end, and a bright rim of emission can be seen in Figure 1(a) to follow the western edge of this lobe as well. Both lobes end in a bright clump of X-ray emission.

4.2 NGC 4649

NGC 4649, also known as M 60, is an E2 galaxy located in a group at the eastern edge of the Virgo cluster. Figure 2 shows our *Chandra*/VLA comparison for NGC 4649. Figure 2(b) shows cavities in the X-ray emission that are coincident with the lobes of the weak radio source. The lobes extend northeast and southwest, along an axis approximately 31 degrees east of north. The northern lobe bends westward, while the southern lobe bends eastward, giving the radio source an overall S shape. The central X-ray source can be seen in Figure 2(b) to have slight bulges along the axis of the radio source. These bulges appear to also be coincident with the axis of the 5 arcsec long central bar found by Randall et al. (2004) in an analysis of *Chandra* data. Randall et al. (2004, 2006) also suggest the existence of "fingers" in the X-ray emission which extend radially from the center of the galaxy. These features are on a much larger
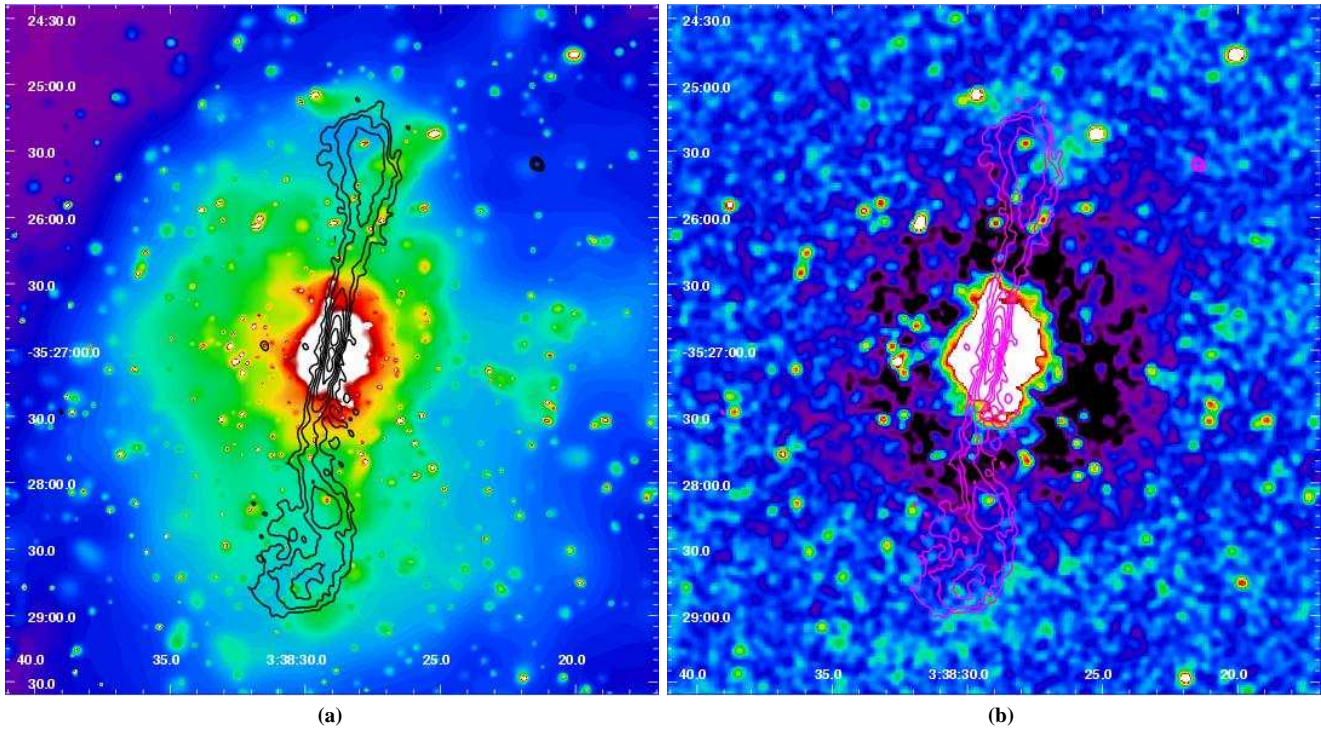
Figure 1. X-ray images of NGC 1399 with 1.4 GHz radio contours. The left panel shows an adaptively smoothed X-ray image with a logarithmic color scale, and the right panel shows an unsharp-masked X-ray image with a linear color scale. The unsharp-masking was done by subtracting a raw image smoothed using an 80 arcsec Gaussian kernel from one smoothed using a 4 arcsec Gaussian kernel. The dark ring in the unsharp-masked image is due to the central source being much brighter than the rest of the image.
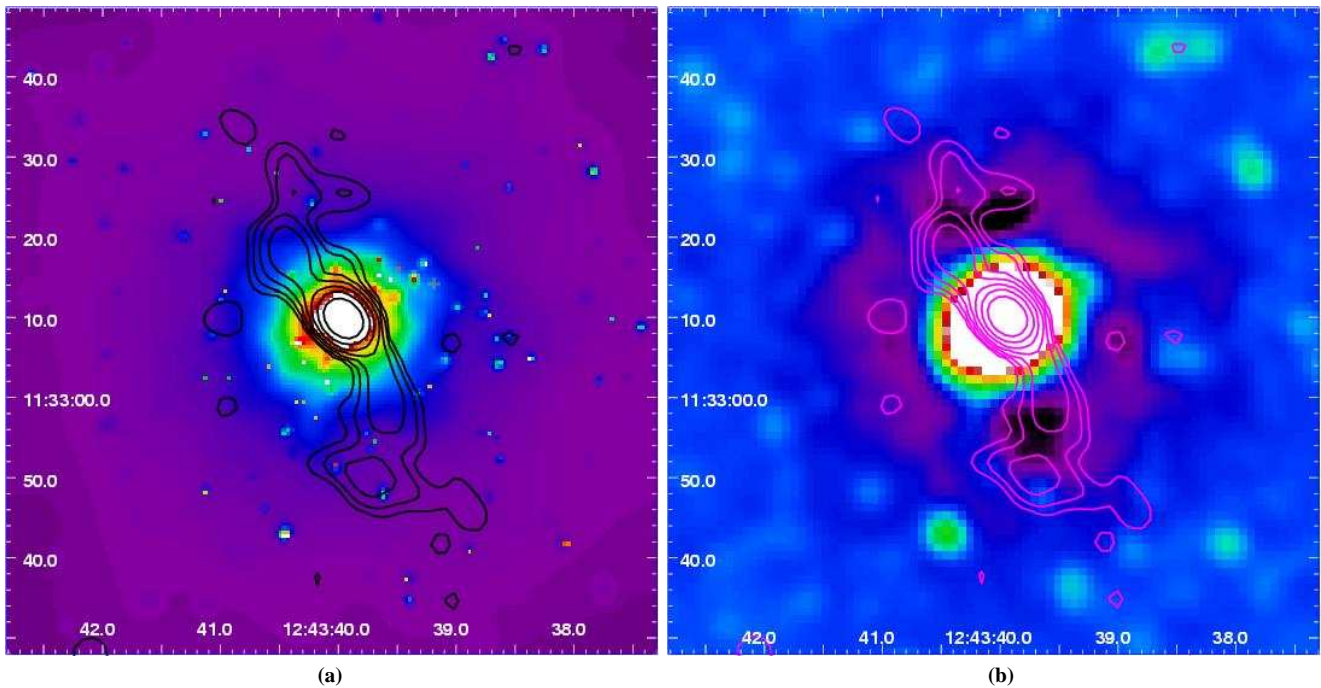
Figure 2. X-ray images of NGC 4649 with 1.4 GHz radio contours. The left panel shows an adaptively smoothed X-ray image with a logarithmic color scale, and the right panel shows an unsharp-masked X-ray image with a linear color scale. The unsharp-masking was done by subtracting a raw image smoothed using a 20 arcsec Gaussian kernel from one smoothed using a 4 arcsec Gaussian kernel.

scale than the radio emission, however, and thus are not present in the region shown in our images. We note that there are several small radio structures at the lowest contour level on the east and west sides of the X-ray source, some of which appear to coincide with depressions in the X-ray images. These are likely to be artifacts, though future observations may aid in determining whether or not they are real features.

4.3 Jet Power

In order to estimate the jet power required to evacuate the observed cavities in the X-ray emitting medium, we employ the method detailed in Allen et al. (2006). Using the radio contours as a guide, we model the cavities as ellipsoids with semi-axis dimensions r_1 along the direction of the jet, r_w across it, and r_d along the line of sight. As the actual depth of the cavities is unknown, we assume symmetry about the axis defined by the direction of the jet, such that $r_d = r_w$. Thus the volume of the cavity is given by $V = 4\pi r_1 r_w^2/3$, though systematic uncertainties in the cavity dimensions cause this value to be uncertain by about a factor of 2. This uncertainty in the volume is taken into account in subsequent calculations. The thermal pressure P at the center of the cavity is determined from temperature and density measurements of the X-ray emitting gas. From these values, we can calculate the $P\,dV$ work done on the X-ray gas by the AGN jets in inflating the cavities. The energy E required for this process is then found by adding the $P\,dV$ work done on the X-ray gas to the internal energy of the cavity:

$$E = P\,dV + \frac{1}{\gamma_2 - 1}PV = \frac{\gamma_2}{\gamma_2 - 1}PV. \tag{1}$$

Here γ_2 is the mean adiabatic index of the relativistic plasma contained in the cavity and has a value of 4/3. Thus the energy of the cavity is given by $E = 4PV$.

The jet power can be estimated using the kinetic energy E of the jet and the age of the cavity. We approximate the age of the cavity as the sound-speed expansion timescale t_{cs}, which is the time required for the cavity to expand to its observed size at the speed of sound in its current environment (see e.g. Dunn, Fabian & Taylor 2005; Bîrzan et al. 2004):

$$t_{cs} = r_1/c_s, \tag{2}$$

where c_s is the local sound speed. The jet power can then be estimated as

$$P_{jet,\,cs} = E/t_{cs}. \tag{3}$$

Because the cavities consist of low density plasma and are thus expected to rise buoyantly through the surrounding medium, the age of the cavity can also be approximated as the buoyancy rise time t_{buoy}, which is the time required for the cavity to rise buoyantly from the center of the galaxy to its current location. The buoyancy velocity is $v_{buoy} = \sqrt{2gV/SC_D}$, where $S = \pi r_w^2$ is the cross-sectional area of the cavity, $C_D \sim 0.75$ is the drag coefficient, and the gravitational acceleration is given by $g = GM(<R)/R^2$. The age, then, is approximately

$$t_{buoy} = R/v_{buoy}, \tag{4}$$

where R is the distance from the center of the black hole to the center of the cavity. The mass profiles used in the calculation of v_{buoy} come from the deprojection of the X-ray data assuming hydrostatic equilibrium. The jet power can be calculated as

$$P_{jet,\,buoy} = E/t_{buoy}. \tag{5}$$

The P_{jet} calculations are summarized in Table 4.

4.4 A Note on the Timescales

We have considered two different timescales in the calculations of jet power: one derived from the local sound speed and the other derived from the buoyancy velocity. The sound speed timescale measures the expansion of the cavity at its current location, and is an appropriate estimate in cases in which the cavities are active, meaning that they are currently powered by the jets of the AGN. The buoyancy timescale, however, measures the rise time of the cavity to its current location, and is an appropriate estimate in the case of cavities that have detached from the core and are rising buoyantly through the surrounding medium. Such is the case for ghost cavities, which are not associated with GHz radio emission.

In the case of NGC 1399, t_{buoy} is on average a factor of 2 greater than t_{cs}. The cavities are fairly well detached from the core, as can be seen in Figure 1. However, they are associated with 1.4 GHz emission and thus are presently powered by the AGN jets. Because the cavities in NGC 1399 are detached but still active, it is difficult to determine which timescale is the most appropriate description for the ages of the cavities in this system. In NGC 4649, the resolution of the radio image does not allow us to determine if the cavities are detached or not, though both timescales are generally in agreement with each other within the errors.

5 PARTICLE ENERGIES AND VOLUME FILLING FRACTIONS

Using the synchrotron emission from the radio lobes, the energy contained within the relativistic electrons can be calculated. Under the assumption that the radio lobes are in pressure balance with their surroundings, their particle content can be investigated. Fabian et al. (2002) studied the lobes of 3C 84 in the Perseus cluster, and subsequently Dunn & Fabian (2004); Dunn, Fabian & Taylor (2005) investigated a large number of radio sources in galaxy clusters. For a more detailed description of the method, see Dunn & Fabian (2004). Here we outline the important details and any changes to that method.

To calculate E_e, the energy in the relativistic electrons, we assume a continuous synchrotron spectrum with a single spectral index α, defined from $S_\nu \propto \nu^\alpha$, between $\nu_1 = 10$ MHz and $\nu_2 = 10$ GHz:

$$E_e = 4\pi \times 10^{12} \left(\frac{cz}{H_0}\right)^2 \left(1 + \frac{z}{2}\right)^2 \frac{S_\nu}{\nu^\alpha} \frac{\nu_2^{0.5+\alpha} - \nu_1^{0.5+\alpha}}{\alpha + 0.5} B^{-3/2}$$
$$\approx aB^{-3/2} \tag{6}$$

(e.g. Fabian et al. 2002). We adopt spectral index values of $\alpha = -0.6$ and $\alpha = -0.7$ for the northern and southern lobes of NGC 4649, respectively (Stanger & Warwick 1986), and $\alpha = -0.92$ for NGC 1399 (Ekers et al. 1989). Also taking into account the energy within the magnetic field, the total energy in the lobes is given by

$$E_{tot} = kE_e + Vf\frac{B^2}{8\pi}, \tag{7}$$

where k accounts for any other particles present in the lobe which are not accounted for by the simplistic model spectrum, V is the volume of the cavity, and f is the volume filling fraction of the relativistic plasma.

The magnetic field present inside the cavity is estimated by comparing the synchrotron cooling time of the plasma to the age of the lobe. The latter can be estimated from the sound-speed expansion timescale or the buoyancy rise time. Under the assumption

Table 4. Summary of the calculation of jet power $P_{\rm jet}$ (in units of 10^{41} erg s^{-1}). "Lobe" refers to the lobe for which the calculation is done (N and S for northern and southern lobe, respectively). R is the distance (in kpc) from the center of the black hole to the center of the cavity, P is the thermal pressure (in eV cm^{-3}) of the X-ray gas at radius R, V is the volume (in cm^3) of the cavity, E is the kinetic energy (in units of 10^{54} erg) of the jets, $t_{\rm cs}$ is the sound speed expansion timescale (in 10^6 yr), and $t_{\rm buoy}$ is the buoyancy rise time (in 10^6 yr).

Source	Lobe	R (kpc)	P (eV cm^{-3})	V (10^{63} cm^3)	E (10^{54} erg)	$t_{\rm cs}$ (10^6 yr)	$t_{\rm buoy}$ (10^6 yr)	$P_{\rm jet,\,cs}$ (10^{41} erg s^{-1})	$P_{\rm jet,\,buoy}$ (10^{41} erg s^{-1})
NGC 1399	N	8.4 ± 0.8	16.0 ± 2.64	1300 ± 535	131 ± 59.2	5.08 ± 0.55	12.6 ± 3.83	8.24 ± 3.70	3.24 ± 1.49
	S	8.4 ± 0.8	16.0 ± 2.65	2950 ± 1210	300 ± 134	6.98 ± 0.76	10.8 ± 3.30	13.7 ± 6.09	8.57 ± 3.93
NGC 4649	N	1.1 ± 0.1	133 ± 28.3	50.0 ± 20.4	41.8 ± 19.7	1.91 ± 0.20	1.32 ± 0.36	6.95 ± 3.26	9.95 ± 4.54
	S	1.3 ± 0.1	134 ± 28.3	43.7 ± 18.0	36.6 ± 17.5	1.94 ± 0.20	1.72 ± 0.48	6.03 ± 2.84	6.63 ± 3.11

that the lobes are in pressure balance with their surroundings, we can obtain upper limits on the ratio k/f:

$$\frac{k}{f} = \left(P - \frac{B^2}{8\pi} \right) \frac{3V}{a} B^{3/2}. \qquad (8)$$

If $k/f = 1$, the lobe is uniformly filled with a purely electron-positron plasma with energies corresponding to emission only in the range of 10 MHz to 10 GHz. If $f \sim 1$ and $k/f > 1$, then $k > 1$, which implies that there are "extra" particles present. These could be thermal protons mixed into the relativistic plasma as the jet travels out from the AGN, or they could be electrons which radiate outside of the assumed spectrum.

We calculate the k/f values using timescales derived from the sound speed, as well as those derived from the buoyancy velocity. These values are presented in Table 5. The equipartition values $k/f_{\rm eq}$ are calculated under the assumption that the plasma within the cavity is at equipartition with the pressure from the surrounding medium. We use a Monte-Carlo algorithm to calculate the uncertainties in the upper limits obtained on k/f. The resulting distribution of limits on k/f is non-gaussian. We find that a log-normal distribution is a fair description of the data, and it is from this that the values for the uncertainties quoted in Table 5 are taken. The values for the uncertainties are large, approximately a factor of 3 of the k/f values.

There is a striking difference between the k/f limits, namely that those of NGC 1399 are much lower than those of NGC 4649. This difference is linked to the radio flux, which is roughly a factor of 20 lower in NGC 4649. The lower the value of k/f, the closer the assumed electron energy spectrum is to the actual one in the lobe. However, as the synchrotron plasma ages, the high energy electrons lose their energy more rapidly, and the distribution of energies shifts to lower energies and also spreads out. Therefore, observing old radio lobes at high frequencies results in low radio fluxes, which, if the spectrum is assumed to be flat, underestimates the number of particles present. As a result, there would be a mismatch between the internal and external pressures. In these calculations we force the lobes to be in pressure balance by increasing k and/or decreasing f.

We currently have a lower cut-off to the synchrotron spectrum of $\nu = 10$ MHz. However, in old lobes there would be very low energy electrons, and so this lower cut-off might be too high. Under the assumption that $k/f = 1$ and that we have correctly modeled the synchrotron spectrum, we calculate the appropriate ν_1. We set an absolute lower limit of the cyclotron frequency appropriate to the magnetic field determined within the radio lobes. For the northern and southern lobes in NGC 1399, $k/f = 1$ can be obtained using a minimum frequency of 265 Hz and 49 Hz respectively (the cyclotron frequencies are 54 Hz and 43 Hz). However, in NGC 4649,

even with the lower cut off at the cyclotron frequency (~ 100 Hz), k/f is 2700 and 890 for the northern and southern lobes respectively.

Another explanation is that the assumed spectrum is close to what exists in the cavity but that there are non-relativistic particles present in the lobes, especially in NGC 4649. Thermal protons could be entrained as the jet travels through the inner parts of the galaxy and halo. These would exert a pressure on the surrounding X-ray gas, but would be undetectable from the radio synchrotron emission.

In NGC 1399, the limits on k/f implies that there are few entrained particles and that the assumed spectrum does describe the distribution of electrons in the lobe reasonably well. However, in NGC 4649 either there are many entrained particles or the model spectrum does not describe the electron population well.

There is close agreement between the limits obtained from the sound speed and buoyancy timescales. We find that the only lobes which can be in equipartition between the leptons and the magnetic field are those from NGC 4649 if the buoyancy timescale is used to calculate the magnetic field from the synchrotron cooling time.

6   CONCLUSIONS

In analyzing *Chandra* and VLA data for NGC 4649, we have found cavities in the surrounding X-ray emitting gas that have not been previously reported. We used these cavities and those in NGC 1399 to estimate the power of the jets emanating from the central black hole of these systems. The $P_{\rm jet}$ values for NGC 1399 using the sound speed expansion timescale are $\sim 8 \times 10^{41}$ erg s^{-1} for the northern lobe and $\sim 14 \times 10^{41}$ erg s^{-1} for the southern lobe. The values using the buoyancy rise time are on average a factor of 2 lower for both lobes, but are roughly in agreement with the aforementioned values within the errors. As the cavities in NGC 1399 are detached from the core but presently powered by the AGN jets, it is difficult to determine which timescale is the relevant one in this case. In NGC 4649, the $P_{\rm jet}$ values using the sound speed expansion timescale are $\sim 7 \times 10^{41}$ erg s^{-1} for the northern lobe and $\sim 6 \times 10^{41}$ erg s^{-1} for the southern lobe. Calculations using the buoyancy rise time yield similar values, within the errors.

Comparing these jet powers to those calculated in Allen et al. (2006), we find that our sources have jet powers that are lower than most of those in their sample. Examples are M 87 and NGC 4696, both of which are located within dense cluster environments. M 87 is near the center of the Virgo cluster and has jet powers which are roughly an order of magnitude larger than those of our sources. The jet powers for the lobes of NGC 4696, which is in the center of Centaurus, are roughly 3 to 4 times those of our sources. We find that our sources have similar jet powers to those of NGC 4552 in

Table 5. k/f values. S is the radio flux (in Jy) of the specified lobe, $k/f_{\rm eq}$ is the equipartition value, $k/f_{\rm sound}$ is calculated using the sound-speed expansion timescale, and $k/f_{\rm buoy}$ is calculated using the buoyancy rise time.

Galaxy	Lobe	S (Jy)	$k/f_{\rm eq}$	$k/f_{\rm sound}$	$k/f_{\rm buoy}$
NGC 1399	N	0.11 ± 0.01	$67.0^{+190}_{-23.6}$	$93.0^{+286}_{-30.3}$	$93.6^{+273}_{-32.2}$
	S	0.13 ± 0.01	$129^{+366}_{-45.8}$	$190^{+531}_{-68.4}$	$177^{+530}_{-59.0}$
NGC 4649	N	0.0038 ± 0.0002	12000^{+33300}_{-4340}	15800^{+40300}_{-6220}	13600^{+47900}_{-3880}
	S	0.0034 ± 0.0002	9450^{+26900}_{-3320}	12400^{+32500}_{-4690}	12000^{+39800}_{-3630}

Virgo, which has values of $\sim 7 \times 10^{41}$ erg s^{-1} and $\sim 8 \times 10^{41}$ erg s^{-1}, as well as those of NGC 5846, which dominates a group of intermediate mass and has jet powers of $\sim 4 \times 10^{41}$ erg s^{-1} for each lobe.

We also investigated the particle content of the cavities by calculating k/f. We find that the k/f values for NGC 4649 are much larger than those of NGC 1399 by about 2 orders of magnitude. Dunn, Fabian & Taylor (2005) found that there is a large range of values for k/f in cavities found in cluster galaxies. In general, k/f is in the range of ~ 1 to ~ 1000 for cavities that are active. The values for NGC 1399 fall into this range; however, in the case of NGC 4649, the values for k/f using either timescale are more than a factor of 10 larger than the upper limit of what has been previously observed.

The minimum value of $k/f = 1$ corresponds to a lobe which is filled with a uniform electron-positron plasma with energies corresponding to emission in the range of 10 MHz to 10 GHz. Large values of k/f, such as those found in NGC 4649, can be achieved by large values for k or small values for f. Large values for k imply that, in order for there to be pressure balance, there must be particles present within the lobe which are not accounted for by the assumed spectrum. These particles can be electrons whose emission is outside the range of 10 MHz to 10 GHz or thermal protons that either exist in the jets during their formation or are entrained as the cavities travel through the surrounding medium. The filling factor f describes the fraction of the volume of the cavity that is occupied by radio emitting plasma. The remaining volume fraction can either be occupied by thermal gas or plasma whose relativistic electrons have aged. Dunn, Fabian & Taylor (2005), in studying ghost cavities as well as active cavities in Centaurus and Perseus, found that the older cavities have larger k/f values than the active ones and have attributed this to the aging of the relativistic electrons.

The k/f values for NGC 4649 are similar to those of ghost cavities in which the relativistic electrons have aged, though the values can also suggest that the the lobes contain entrained particles. If the electrons in the lobes of NGC 4649 have aged, the model spectrum is simply not an accurate description of the electron distribution. This scenario seems likely, as the radio flux is so small that NGC 4649 is expected to soon become a ghost cavity system should clear cavities remain. For NGC 1399, the model spectrum appears to be an appropriate description of the lobe contents, and there are probably not many entrained particles. As was proposed by Dunn & Fabian (2004), higher power radio sources are less likely to pick up extra particles from the surrounding medium. Our results agree with this description in that NGC 1399 has lower k/f values than NGC 4649 and also higher radio power. However, there are many physical parameters to consider in investigating these values, and no clear correlation has been found between k/f and any one parameter.

In calculating k/f we have assumed a simple power-law spectrum. Using high frequency observations to obtain radio flux mea-

surements of a lobe whose relativistic electrons have aged would tend to cause this power-law approximation to underestimate the energy of the relativistic electrons in the lobe and therefore overestimate k/f. Our results, then, could be said to suggest that the lobes in NGC 4649 are likely to be older than those in NGC 1399. However, these results could also suggest that the power-law approximation may be poor in both cases. In order to determine whether the power-law assumption is reasonable, it would be desirable to obtain sensitive lower frequency VLA observations of these galaxies, such as at 330 MHz, that would allow for accurate measurements of the radio flux in the regions corresponding to the cavities.

REFERENCES

Allen S. W., Dunn R. J. H., Fabian A. C., Taylor G. B., Reynolds C. S., 2006, MNRAS, 372, 21

Arnaud K. A., 1996, in Jacoby G. H., Barnes J., eds, ASP Conf. Ser.101: Astronomical Data Analysis Software and Systems V XSPEC: The First Ten Years. p.17

Bernardi M., Hyde J. B., Sheth R. K., Miller C. J., Nichol R. C., 2006, astro-ph/0607117

Best P. N., Kauffmann G., Heckman T. M., Brinchmann J., Charlot S., Ivezić Ž., White S. D. M., 2005, MNRAS, 362, 25-40

Best P. N., von der Linden A., Kauffmann G., Heckman T. M., Kaiser C. R., 2006, astro-ph/0611197

Beuing J., Dobereiner S., Böhringer H., Bender R., 1999, MNRAS, 302, 209

Bîrzan L., Rafferty D. A., McNamara B. R., Wise M. W., Nulsen P. E. J., 2004, ApJ, 607, 800

Böhringer H., Voges W., Fabian A. C., Edge A. C., Neumann D. M., 1993, MNRAS, 264, L25

Bondi H., 1952, MNRAS, 112, 195

Churazov E., Brüggen M., Kaiser C. R., Böhringer H., Forman W., 2001, ApJ, 554, 261

Condon J. J., Cotton W. D., Greisen E. W., Yin Q. F., Perley R. A., Taylor G. B., Broderick J. J., 1998, AJ, 115, 1693

Di Matteo T., Allen S. W., Fabian A. C., Wilson A. S., Young A. J., 2003, ApJ, 582, 133

Diehl S., Statler T. S., 2006, astro-ph/0606215

Donahue M., Horner D. J., Cavagnolo K. W., Voit G. M., 2006, ApJ, 643, 730

Dunn R. J. H., Fabian A. C., 2004, MNRAS, 355, 862-873

Dunn R. J. H., Fabian A. C., Taylor G. B., 2005, MNRAS, 364, 1343

Dunn R. J. H., & Fabian A. C., 2006, MNRAS, 373, 959

Ebeling H., White D. A., Rangarajan F. V. N., 2006, MNRAS, 368, 65

Ekers R. D., Wall J. V., Shaver P. A., Goss W. M., Fosbury R. A. E., Danziger I. J., Moorwood A. F. M., Malin D. F., Monk A. S., Ekers J. A., 1989, MNRAS, 236, 737

Fabian A. C., Celotti A., Blundell K. M., Kassim N. E., Perley R. A., 2002, MNRAS, 331, 369

Fabian A. C., Sanders J. S., Allen S. W., Crawford C. S., Iwasawa K., Johnstone R. M., Schmidt R. W., Taylor G. B., 2003, MNRAS, 344, L43

Fabian A. C., Sanders J. S., Ettori S., Taylor G. B., Allen S. W., Crawford C. S., Iwasawa K., Johnstone R. M., Ogle P. M., 2000, MNRAS, 318, L65

Fabian A. C., Sanders J. S., Taylor G. B., Allen S. W., Crawford C. S., Johnstone R. M., Iwasawa K., 2006, MNRAS, 366, 417

Fanaroff B. L. & Riley J. M., 1974, MNRAS, 167, 31P

Finoguenov A., & Jones C., 2001, ApJ, 547, L107

Forman W., Nulsen P., Heinz S., Owen F., Eilek J., Vikhlinin A., Markevitch M., Kraft R., Churazov E., Jones C., 2005, ApJ, 635, 894

Mahdavi A., Geller M. J., 2001, ApJ, 554, L129

McNamara B. R., Wise M., Nulsen P. E. J., David L. P., Sarazin C. L., Bautz M., Markevitch M., Vikhlinin A., Forman W. R., Jones C., Harris D. E., 2000, ApJ, 534, L135

Mewe R., Kaastra J. S., Leidahl D. A., 1995, Legacy, 6, 16

O'Sullivan E., Forbes D. A., Ponman T. J., 2001, MNRAS, 328, 461

Paolillo M., Fabbiano G., Peres G., Kim D.-W., 2002, ApJ, 565, 883

Randall S. W., Sarazin C. L., Irwin J. A., 2004, ApJ, 600, 729

Randall S. W., Sarazin C. L., Irwin J. A., 2006, ApJ, 636, 200

Rafferty D. A., McNamara B. R., Nulsen P. E. J., Wise M. W., 2006, ApJ, 652, 216

Stanger V. J., & Warwick, R. S., 1986, MNRAS, 220, 363

Taylor G. B., Fabian A. C., Allen S. W., 2002, MNRAS, 334, 769

Taylor G. B., Sanders J. S., Fabian A. C., Allen S. W., 2006, MNRAS, 365, 705

Tremaine S., Gebhardt K., Bender R., Bower G., Dressler A., Faber S. M., Filippenko A. V., Green R., Grillmair C., Ho L. C., Kormendy J., Lauer T. R., Magorrian J., Pinkney J., Richstone D., 2002, ApJ, 574, 740

Wegner G., Bernardi M., Willmer C. N. A., da Costa L. N., Alonso M. V., Pellegrini P. S., Maia M. A. G., Chaves O. L., Rité C., 2003, AJ, 126, 2268